Ocean Dynamics (2016) 66:1517–1527
DOI 10.1007/s10236-016-0992-5

Surface suspended particulate matter concentration in the Taiwan Strait during summer and winter monsoons

Jason C. S. Yu[1] · **Tzu-Yin Chou**[1] · **Hao-Cheng Yu**[1] · **Peihung Chen**[1] · **Quinten Vanhellemont**[2] · **Michael Fettweis**[2]

Received: 31 January 2016 / Accepted: 6 September 2016 / Published online: 22 September 2016

Abstract The Taiwan Strait (TS), situated between Taiwan and China, is shallow, relatively turbid, and characterized by strong tidal currents and winter and summer monsoon seasons. The aim of this study was to use images from the Moderate Resolution Imaging Spectroradiometer (MODIS) on board the Aqua satellite to investigate how local sediment sources in addition to the seasonality in wind, oceanographic currents, and waves influence the suspended particulate matter (SPM) dynamics in the TS. In winter, northeast (NE) winds drive the China Coastal Current southward. Cold water with a high SPM concentration is transported southward into the Strait. After the highest SPM concentration reaches its peak in December and January, the winds weaken and the SPM concentration decreases. During summer, winds are less strong and SPM concentration is lower. Although typhoons typically occur in summer, they generate only a weak signal in the surface SPM concentration data from MODIS because of the low number of cloud-free images during these periods. Typhoons result in a short-term increase in the SPM concentration but do not strongly influence the seasonal values in the satellite-derived SPM concentration maps.

This article is part of the Topical Collection on the *13th International Conference on Cohesive Sediment Transport in Leuven, Belgium 7–11 September 2015*

Responsible Editor: Joris Vanlede

✉ Jason C. S. Yu
jasonyu@mail.nsysu.edu.tw

[1] Department of Marine Environment and Engineering, National Sun Yat-Sen University, Lien-Hai Road 70, 80424 Kaohsiung, Taiwan

[2] Royal Belgian Institute of Natural Sciences, Operational Directorate Natural Environment, Gulledelle 100, B-1200 Brussels, Belgium

Keywords Suspended particulate matters · Monsoon · Seasonal variation · Taiwan Strait

1 Introduction

Coastal seas are often characterized by high variability in the concentration of suspended particulate matter (SPM) (Schoellhamer 2002; Liao et al. 2008; Liu et al. 2008; Fettweis et al. 2012). The predominant forces that cause such variations are related to tides, waves, and meteorological and seasonal variations and influences (Jan et al. 2002). The Taiwan Strait (TS) connects the South China Sea (SCS) with the East China Sea (ECS) and covers an area of approximately 6300 km^2 (Fig. 1). The mean transport through the TS is approximately 1.8 Sv and is directed northward. The maximum transport occurs during summer (2.7 Sv) and the minimum during winter (0.9 Sv) (Jan et al. 2004; Lin et al. 2000; Wang et al. 2003). The TS is shallow (average water depth approximately 50 m) and relatively turbid; it has strong tidal currents (average tidal current approximately about 0.4 ms^{-1}) and typical winter and summer monsoon seasons (Jan et al. 2002; Chen and Wang 2006; Qiu et al. 2011). The most notable high-turbidity areas are situated along the Chinese and Taiwanese coasts, as well as in the shallow parts of the TS such as the Changyun Ridge and Taiwan Bank (Fig. 1). The seasonal wind pattern (Fig. 2) is characterized by southwesterly winds in summer and northeast (NE) winds in winter that determine not only the residual ocean currents and the transport of SPM but also the input of SPM from rivers into the TS as well as the local resuspension induced by waves (Hoefel and Elgar 2003; Bai et al. 2015). During winter (November to February), monsoon winds generally blow from the NE and direct the cold China Coastal Current (CCC) toward the SW. The 20 °C isotherm shows the intrusion of these waters into

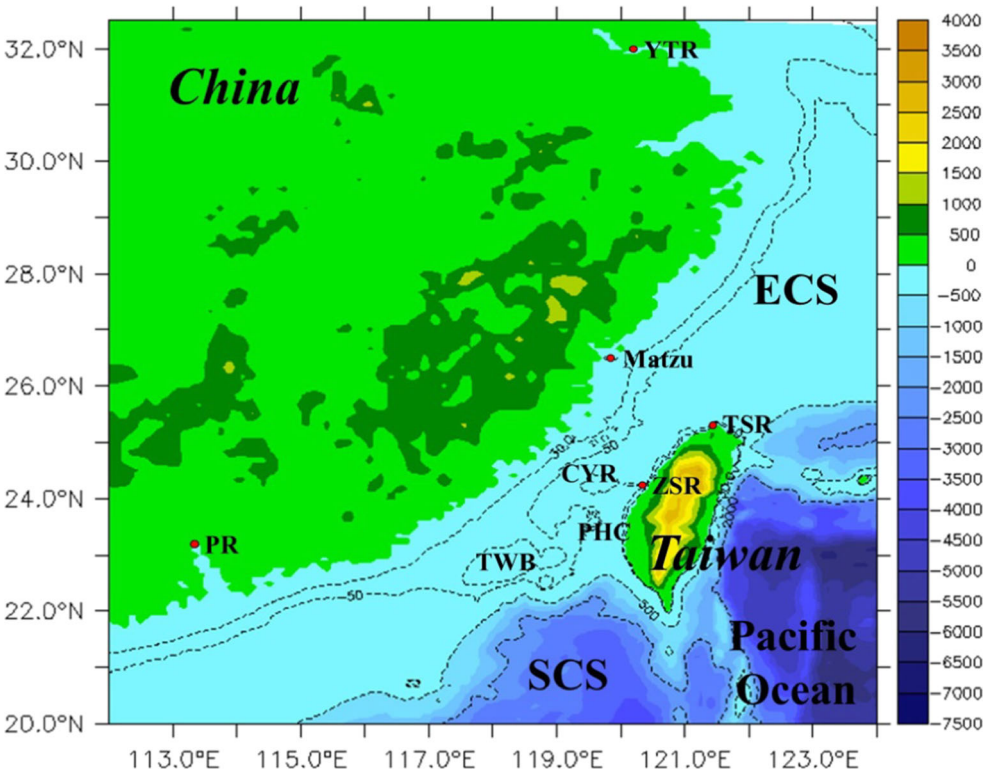

Fig. 1 Bathymetry and topography (m) around Taiwan. *CYR* Changyun Ridge, *ECS* East China Sea, *PHC* Penghu Channel, *SCS* South China Sea, *TWB* Taiwan Bank, *TSR* Tanshui River, *YTR* Yangtze River, *ZSR* Zhuoshui River

the TS from December to March, where they meet the Kuroshio branch at Penghu Channel (Fig. 3). The CCC is further blocked by Changyun Ridge, where it deviates toward the NE. During the summer monsoon season (June–September), the SW winds advect the South China Sea surface current (SCSSC) warm water from the SW through the Penghu Channel into the ECS (Fig. 3) (Hong et al. 2009; Jan et al. 2002; Qiu et al. 2011). These SW winds induce heavy rainfall, which is most pronounced during typhoon overpasses, resulting in high river discharges into both sides of the TS and a large input of fine-grained sediments into the strait that are rapidly dispersed (Dadson et al. 2005; Liu et al. 2006; Chien et al. 2011). Larger-scale SPM transport patterns are associated with the sediment input from large rivers and prevailing ocean currents. The sediments discharged by the Pearl River are transported during summer by the SCSSC along the Chinese coast into the TS (Bai et al. 2015). In winter, southward transport of SPM associated with the CCC occurs, mainly the Yangtze River into the TS (DeMaster et al. 1985; Song and Chen 1992; Xu et al. 2009; Bai et al. 2015).

Most studies on SPM transport in TS have focused on the prominent effects of typhoons (e.g., Milliman and Kao 2005; Chien et al. 2011; Li et al. 2015), whereas general SPM concentration patterns have received less attention. Therefore, the

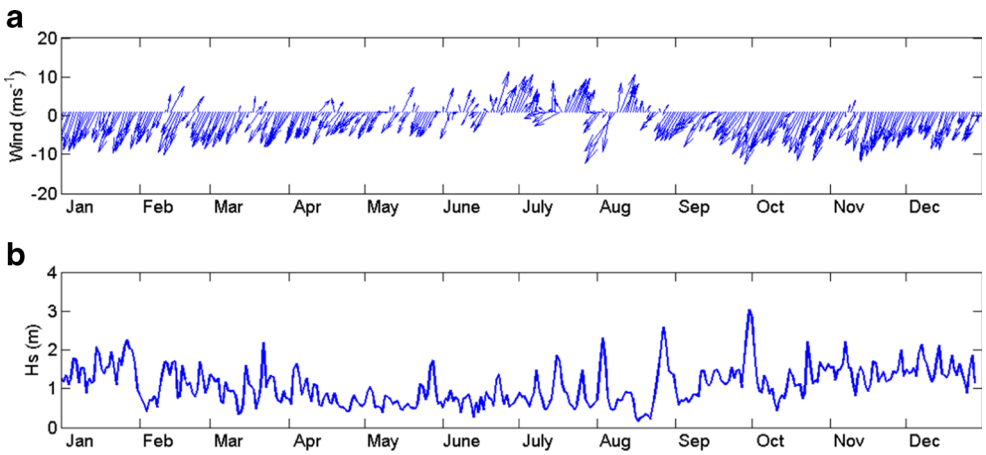

Fig. 2 **a** Surface wind velocities from NASA PO.DAAC (Atlas et al. 2011) and **b** significant wave heights from Taiwan Central Weather Bureau SWAN operational result in 2011 at Matzu (119.92°E, 26.17°N)

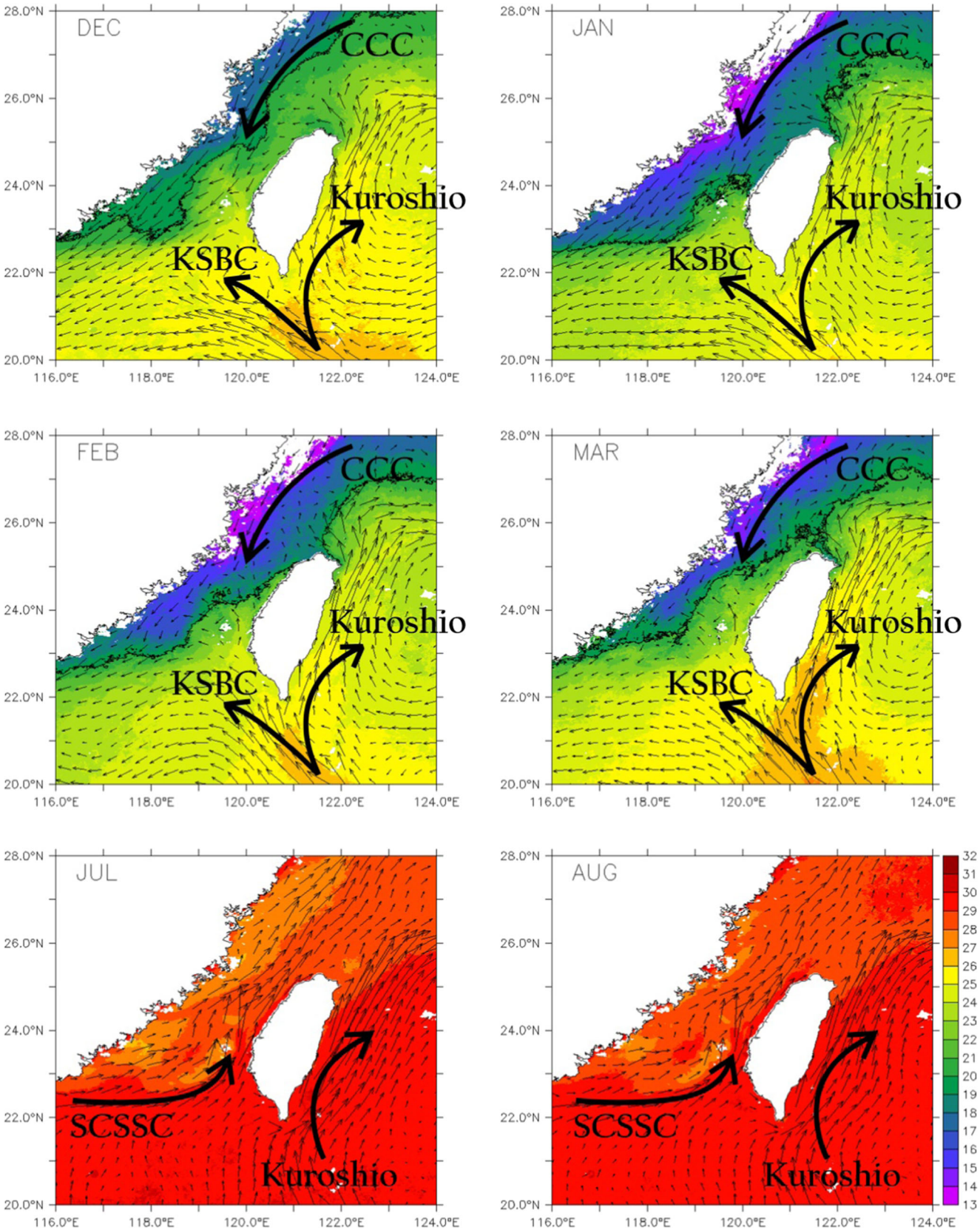

Fig. 3 Monthly averaged surface temperature (°C) composed from MODIS in winter (December to March 2003–2012) and summer (July and August 2003–2012) together with the 2011 HYCOM ocean currents (ms^{-1}). The 20 °C isotherm is shown in *black* (only shown for winter months)

present research focused on the large-scale geographical variability of the high-turbidity zones in the TS that are induced by seasonal meteorological variations and extreme events. This study used images from the Moderate Resolution Imaging Spectroradiometer (MODIS) on board the Aqua satellite (part of the NASA Earth Observing System) to investigate how local sediment sources in addition to the seasonality in wind, oceanographic currents, and waves influence the SPM dynamics in the TS. Polar orbital satellites such as Aqua with MODIS on board cannot be used to assess SPM concentration variations on short time scales because the sampling frequency is too low (once a day) and clouds often obscure the ocean surface. However, averaging of the data according to typical meteorological patterns, months, or seasons results in synoptic maps that are representative of the mean SPM concentration under specific conditions (Fettweis and Nechad 2011; Fettweis et al. 2012).

2 SPM concentration and hydrodynamic data

The MODIS provides one to two daily images. The data are used to design daily maps of the SPM concentration. In total, 4094 MODIS images, covering the period between July 2002 and September 2013, were processed using SeaDAS software (version R2013.0) from level 1A to level 2. The images were collocated on a common rectangular grid by using nearest-neighbor resampling, and multiple overpasses were combined into a single daily composite (Vanhellemont et al. 2011; Vanhellemont and Ruddick 2011). The surface SPM concentration was then retrieved from remote sensing reflectance at the MODIS band centered at a wavelength of 667 nm, using the algorithm of Nechad et al. (2010). Finally, level 2 processing flags (Patt et al. 2003) were used to mask out the land and cloud pixels and any low-quality pixels. The accuracy of the satellite-derived SPM concentration was assessed for errors that may have arisen from the optical model used for converting marine reflectance to SPM concentrations. The model parameterized the inherent optical properties of particles in suspension as site-averaged coefficients. This induces errors in SPM estimation when a significant change in particle size and composition occurs under tidal and wind effects (Nechad et al. 2010), changing significantly their mass-specific inherent optical properties. The uncertainty in SPM concentrations propagating from errors in the water-leaving reflectance retrieval was evaluated for the southern North Sea on the basis of 29 matchups taken in clear to moderately turbid waters (3–80 mg L^{-1}). A mean relative error of approximately 37 % was found in SPM concentration retrieval from MODIS imagery. For waters with an SPM concentration >10 mg L^{-1}, the relative errors in MODIS-derived SPM concentrations are significantly lower than in clearer waters. This is due to higher relative errors in water-leaving reflectance being retrieved in clearer waters and the SPM concentration algorithm being adapted to turbid waters. However, satellite-visible bands typically saturate in extremely turbid waters (Doxaran et al. 2002). The band centered at a wavelength of 667 nm and used in the retrieval of SPM concentration reached its maximum limit of detection at approximately 80 mg L^{-1}; in the data treatment, only pixels with an SPM concentration in this range were analyzed further. Using the red band is appropriate for the TS, where extremely turbid waters occur only near the coast. The near-coast pixels were, however, masked after atmospheric correction because of uncertainties associated with water turbidity, adjacency, and stray light effects.

Additional uncertainty may be due to the Nechad et al. (2010) algorithm, which has been validated for the southern North Sea, being applied to another region (Dogliotti et al. 2015; Han et al. 2016). The uncertainty originated from the reflectance-SPM concentration calibration that inherently includes information on the particle type and size distribution, properties that may vary in space and time. Dogliotti et al. (2015) indicated out that the single-band semi-analytical algorithm (Nechad et al. 2010) and a switching scheme can be used to retrieve turbidity from water reflectance in distinct regions. Turbidity can be converted to SPM concentration and vice versa by applying a constant scaling factor. To our knowledge, no data set is available for the TS to calculate this scaling factor; hence, the SPM concentration in the TS might have a higher uncertainty than that in the southern North Sea. This does not, however, influence the conclusions of SPM dynamics in the TS.

Significant wave heights were calculated for 2011 by using the Simulating WAves Nearshore (SWAN) model with a 0.05° resolution, which is run operationally at the Central Weather Bureau (CWB). The meteo input for SWAN was derived from CWB Weather Research and Forecasting model products. The sea surface currents in the area between 116°E–124°E and 20°N–28°N are from the hybrid coordinate ocean model (HYCOM) global reanalysis operational data (Cummings 2006; Cummings and Smedstad 2013; Fox et al. 2002). The in situ rainfall and river discharge data were obtained from the Water Resources Agency, Taiwan (WRA 2016).

The surface SPM concentration data in addition to wind, wave, and current data from HYCOM and numerical models (Yu et al. 2014) were used to reconstruct the SPM dynamics. The data were ensemble averaged according to winter and summer monsoon weather types.

3 Results and discussion

The monthly distribution of surface SPM concentrations along the Chinese coast and Taiwanese west coast is shown in Fig. 4. The most prominent high-turbidity areas are along the

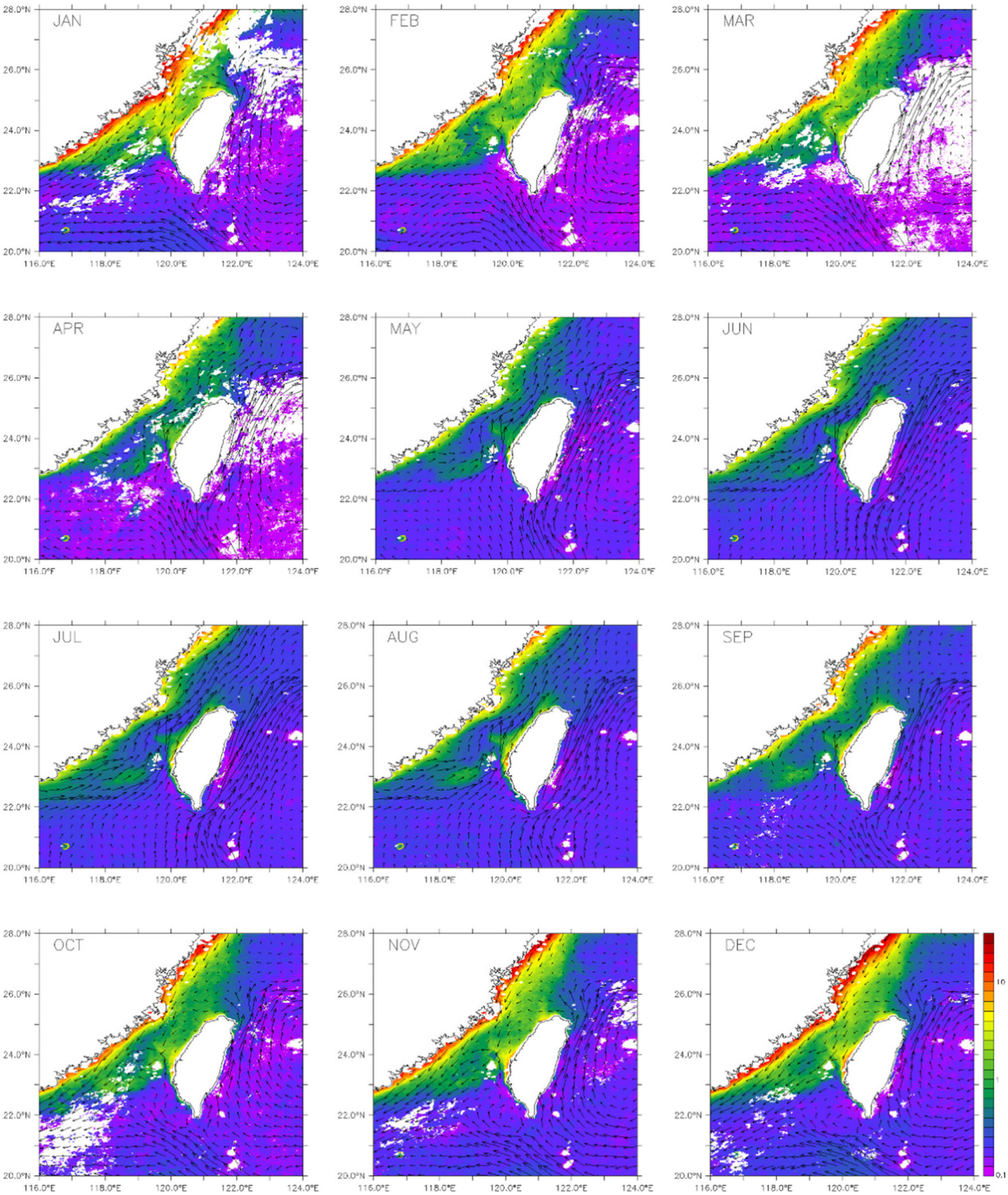

Fig. 4 Monthly averaged (2003–2012) surface SPM concentration (mg L^{-1}) with 2011 residual current (ms^{-1}) (Yu et al. 2014)

Chinese and Taiwanese coasts, in shallow parts of the TS such as the Changyun Ridge and Taiwan Bank, and in Tanshui River and Zhuoshui River plumes. The SPM concentration is highest in December and January, after which it decreases gradually and reaches a minimum between May and August. The SPM concentration drops to low values in the central

parts of the TS, Tangshui River, Zhuoshui River, and Changyun Ridge. The maps clearly show seasonal patterns consistent with a winter season from December to February with high SPM concentrations (i.e., >5 mg L^{-1}) in the whole TS and patterns consistent with a summer season from June to September with high SPM concentrations remaining only in the coastal and shallow areas (Fig. 5).

3.1 Seasonal variations

The surface SPM concentration maps indicate the significant differences between winter and summer monsoon seasons (Fig. 5). The SPM concentration reaches approximately 14 mg L^{-1} in winter and 4 mg L^{-1} in summer at Matzu. These differences are mainly due to the higher wind velocities, wave heights in winter, and inputs of SPM from remote sources, rather than the occurrence of extreme events, such as typhoons, typically associated with summer. The main remote sources are the Pearl River and Yangtze River and other rivers located upstream of the TS during summer and winter, respectively. The SPM annual fluxes from the Yangtze River are higher (478×10^6 t) than those from the Pearl River, estimated at 30 million tons (Milliman and Meade 1983; Wang et al. 2014). In the TS, the NE wind reaches velocities up to 11 ms^{-1} and the residual currents up to 0.7 ms^{-1}, whereas the SW wind occurring during summer (0.5 ms^{-1}) and the residual current velocity (0.4 ms^{-1}) are less strong. The average wave heights during winter are approximately 1.1 m, which are higher than the annual average of 0.8 m. From the 2011 time series in the Tanshui River and Zhuoshui River (Fig. 6), a high SPM concentration corresponds generally with stronger winds and higher wave heights. The associated weaker southwest winds and lower wave heights result in generally lower SPM concentrations in summer than in winter. For the 2003–2010 averages, the correlation between the SPM concentration and wind velocity is moderately high at Matzu (R^2 = 0.53), and at Penghu (R^2 = 0.42) in winter, but lower at other locations in the southern TS. The NE wind dominates the whole TS (Fig. 2), and the waves are responsible for the increase in SPM concentrations, especially in shallow areas (Fig. 2). SPM concentrations are generally low in summer because the wind velocity is low (Fig. 6). Local resuspension is thus mainly dominated by tidal currents rather than waves.

The higher wind speeds and stronger residual currents result in a higher transport of SPM from the extremely turbid Yangtze estuary toward the SW. The higher waves result in higher suspension of fine-grained sediments, leading to a further increase of the surface SPM concentration. The SPM concentration distribution in the TS is clearly limited in the south and the north by the low turbid Kuroshio Ocean current. After the monsoon transition period in May, south or SW winds dominate the wind climate from June to August. The winds generate the SCSSC from south to north, and suspended sediments from the Pearl River estuary flow into the TS (Bai et al. 2015). The lower wind velocities, wave heights, surface residual currents in summer, and the SPM input from the Pearl River (30×10^6 t), compared with the Yangtze River, result in SPM concentrations that are lower than those in winter. Nevertheless, the high SPM concentration areas are still situated along the coast and in shallow area.

3.2 Effects of extreme events

The summer is typically associated with short periods of heavy rain often associated with typhoons, during which large amounts of sediment may enter the TS through mountain

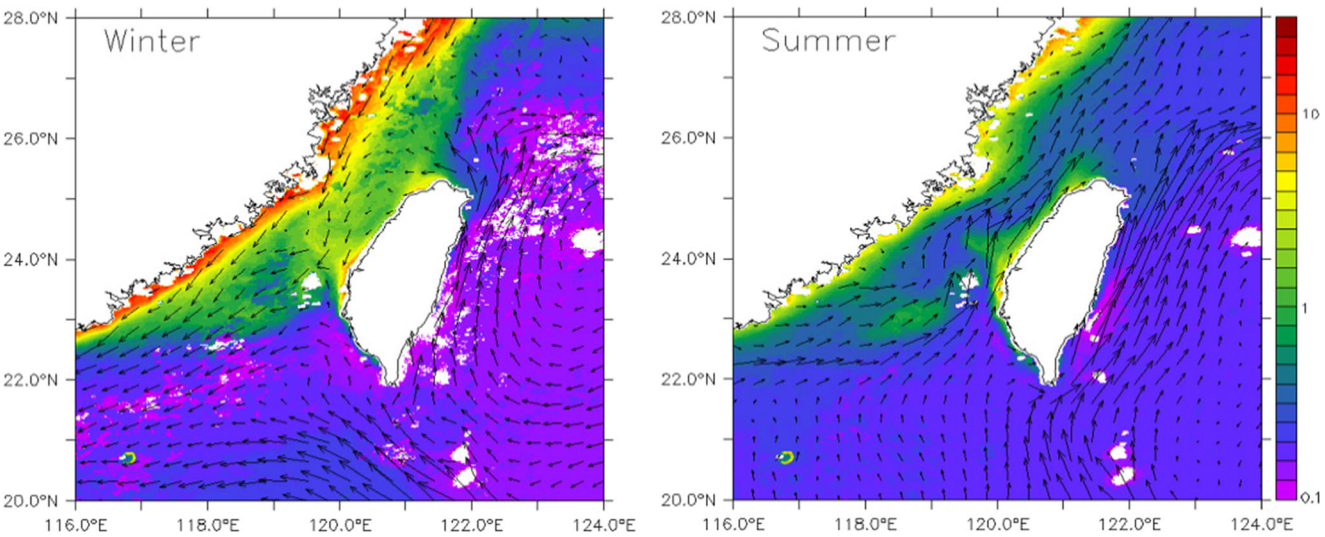

Fig. 5 The averaged (2003–2012) surface SPM concentration (mg L^{-1}; *color layer*) and the residual current velocity (ms^{-1}; *vectors*) in winter (December 2010–February 2011) and summer (June–September 2011)

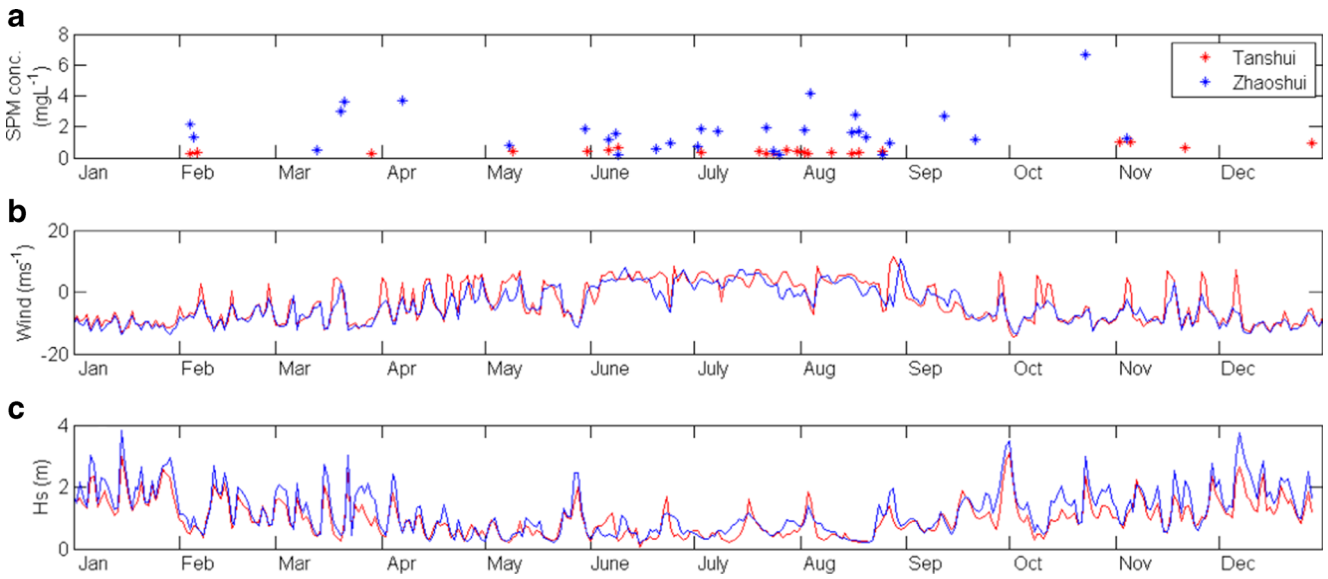

Fig. 6 The 2011 data at Tanshui and Zhuoshui River mouth. **a** Surface SPM concentrations (mg L^{-1}) from MODIS, **b** surface wind velocities (ms^{-1}; *positive values* are SW and *negative* NE winds) from NASA PO.DAAC (NASA/GSFC/NOAA (2009); Atlas et al. 2011), and **c** significant wave height (m) from Taiwan Central Weather Bureau SWAN operational result

rivers in Taiwan. For example, during Typhoon Herb (1996), the Kaoping River in the south of Taiwan discharged 32×10^6 t of sediments, and during Typhoon Kalmaegi (2008), the Zhuoshui River discharged approximately 77×10^6 t in 1 day (Milliman and Kao 2005; Chien et al. 2011), which is larger than the average annual sediment discharge of $40 \pm 6 \times 10^6$ t (Kao and Milliman 2008). The enormous sediment loads during short periods result in high SPM concentration at the river mouth. Chien et al. (2011) mentioned that most of the river runoff was entrained by the alongshore flow instead of jetting directly into the TS. These extreme events are not apparent in the seasonal or monthly

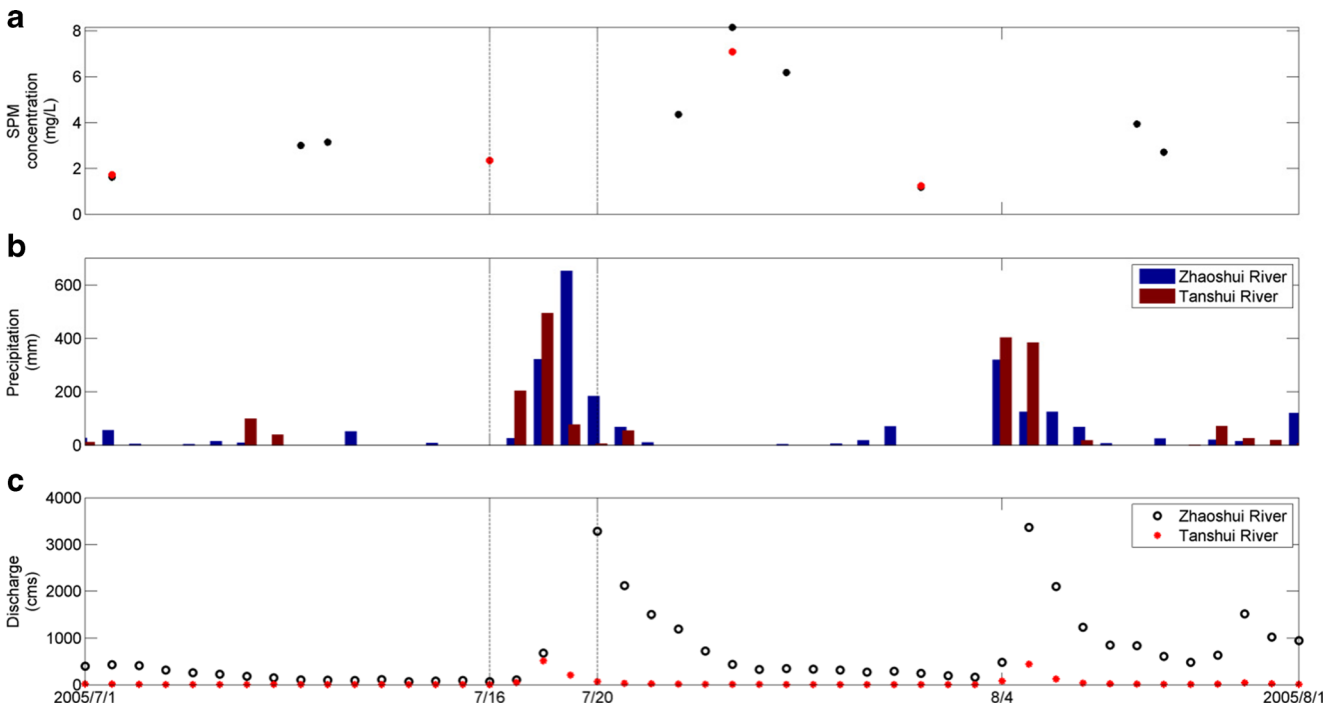

Fig. 7 Typhoon Haitang (2005). **a** Surface SPM concentration from MODIS, **b** precipitation, and **c** river discharge at Zhuoshui and Tanshui river mouth (Fig. 1) during the periods of 1–15 July (T1 pre-typhoon), 16–20 July (T2 actual typhoon), 21 July–4 August (T3 post-typhoon), and 5–19 August (T4 post-typhoon)

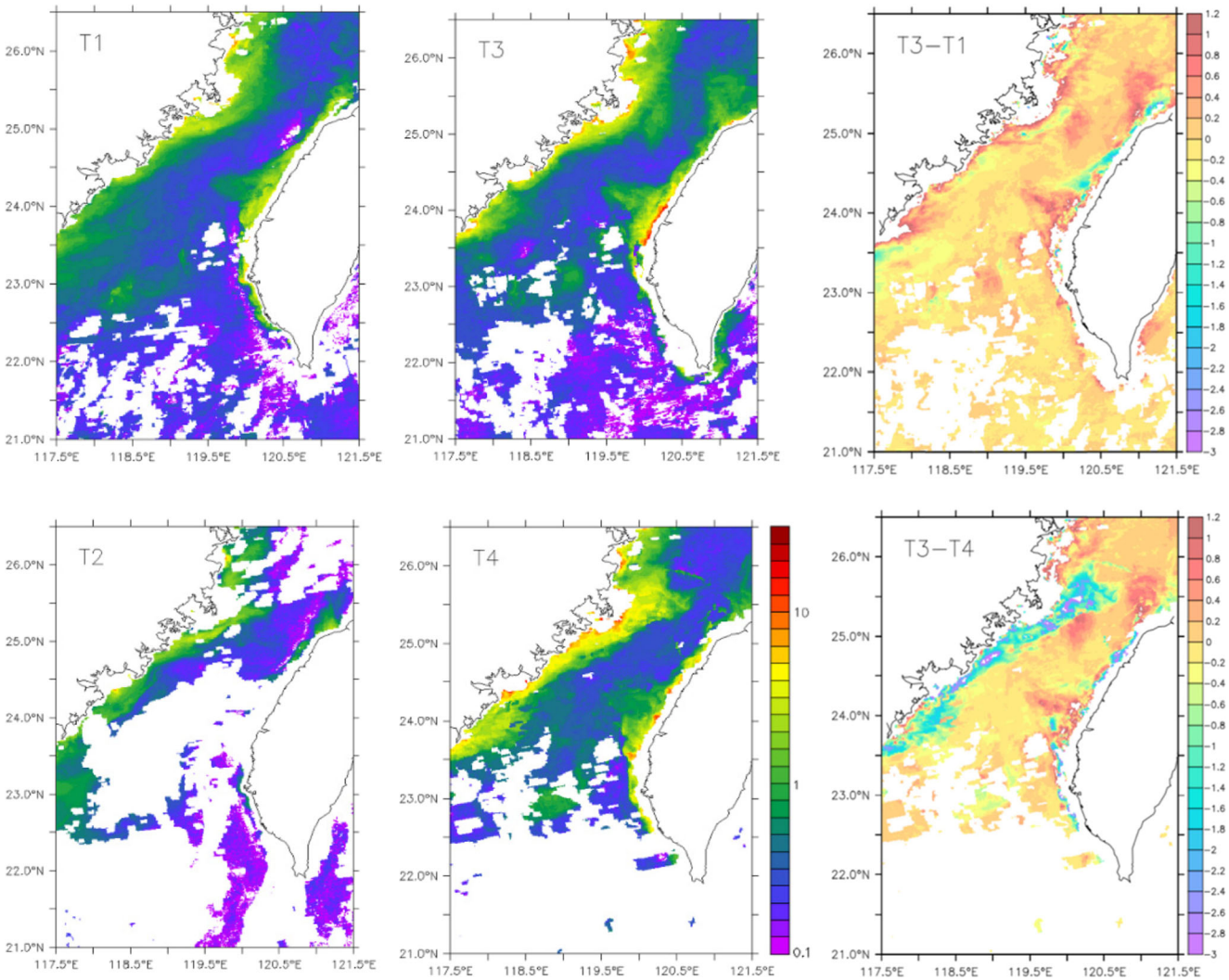

Fig. 8 Typhoon Haitang (2005). Surface SPM concentration (mg L^{-1}) averaged over T1 (pre-typhoon, 1–15 July), T2 (actual typhoon, 16–20 July), T3 (post-typhoon, 21 July–4 August), and T4 (no influential period, 5–19 August) periods, respectively. In addition, the difference in SPM concentration (mg L^{-1}) between periods T3-T1 and T3-T4 is shown (*negative values* means that T1 and T4 have higher SPM concentrations than T3, respectively)

surface SPM concentration maps because the SPM that discharges into the TS probably settles quickly (thus, it can be only partially detected at the surface by the satellite) and because typhoon periods are too cloudy for obtaining representative data of SPM concentration. Below, both hypotheses are discussed in more detail.

Typhoon Haitang (2005) was chosen to investigate the influence of extreme events on the surface SPM concentration detected by MODIS. The increase in SPM concentration was caused by an enormous input of riverine SPM into the TS associated with heavy rainfall and a high river discharge (Fig. 7). A high correlation ($R^2 > 0.8$) can be found between the SPM concentrations at the mouth of Zhuoshui River and both the rainfall and river discharge. Satellite images during a pre-typhoon (T1 1–7 July), actual typhoon (T2 16–20 July), and two post-typhoon periods (T3 21 July–4 August and T4 5–19 August) are shown in Fig. 8. In the pre-typhoon period, the surface SPM concentration is highest at the shallow Changyun Ridge. During the typhoon, no data are available that enable clarification, because of cloud coverage. After the typhoon, the SPM concentration is higher at the Changyun Ridge (approximately 5 mg L^{-1}) and the Zhuoshui estuary (approximately 11 mg L^{-1}) than during the pre-typhoon period (Fig. 8), indicating that the effect of the typhoon on the surface SPM concentration can be detected in the satellite images. After approximately 1 month, after the passage of the typhoon (T4), the SPM concentration difference (T3-T4, -0.2 ± 0.8 mg L^{-1} with 75,728 good data) is similar to that during the pre-typhoon period (T3-T1, 0.1 ± 0.5 mg L^{-1} with 115,003 good data), showing that the SPM concentration increase was dispersed away by the currents or by the settling of the SPM particles (Fig. 8). Because the frequency of typhoons

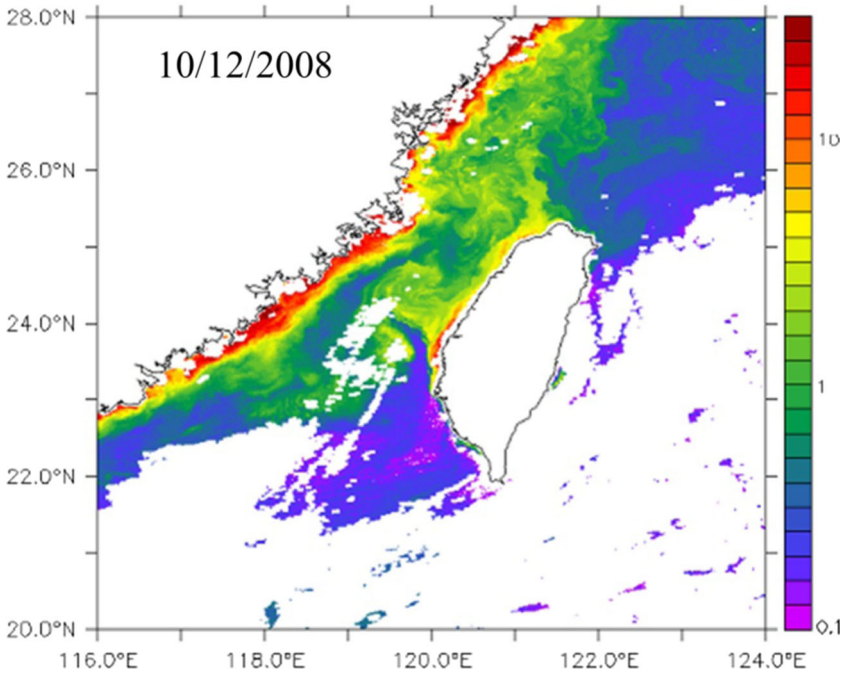

Fig. 9 Surface SPM concentration (mg L^{-1}) from MODIS on 10 December 2008

is low (approximately three typhoons per year), their influence on the seasonal surface SPM concentration pattern is only limited.

3.3 Limitation of satellite imagery

The main drawback of satellite images is related to the low sampling frequency (daily) and the occurrence of clouds. The image from 10 December 2008 (Fig. 9) remains an exception for the TS because it is one of the few cloud-free images of the whole area. The image clearly shows the detailed surface patterns of SPM concentrations that are associated with mesoscale eddies in the surface currents. Averaging the images over periods of months to seasons enables these detailed features to be smoothed out and disappear. Nevertheless, ensemble averaging remains a more appropriate method for determining the SPM dynamics because cloud-free data are limited. The frequency of cloud-free data is higher in summer than in winter (Fig. 10). Furthermore, most of the cloud-free data in winter are from the low-turbidity areas located in southern Taiwan and along the SCS coast (Fig. 10). The results emphasize that the satellite data reflect a lower variability than what could be derived from continuous time series (Fettweis and Nechad 2011).

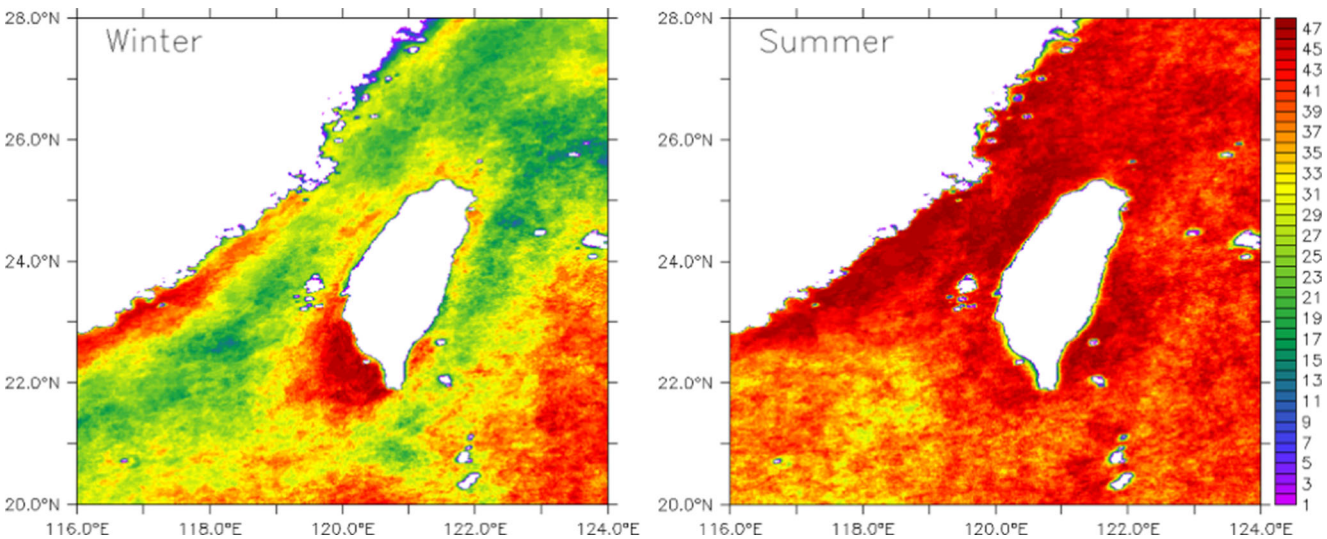

Fig. 10 Number of cloud free pixels in winter and summer during the period of 2003–2012

4 Conclusion

In winter, NE winds drive the CCC southward, and SPM gathers in the TS along the coast and in the estuaries. From September, the NE winds strengthen and change the current direction. SPM is transported southward with the cold water. After the SPM concentration reaches its peak in December, the winds weaken and the SPM concentration decreases after February. The waves induced by NE winds resuspend the fine-grained sediments on the ECS continental shelf and in the TS and transport it southward. However, in summer, the tidal currents are more important than the ocean currents, because the SCSSC forced by southwest winds is weaker than the China Coastal Current forced by NE winds. The movement of tidal currents is responsible for most of the sediment transport in the shallow coastal areas and resuspension at the Penghu Channel and Changyun Ridge. The extreme conditions generate a weak signal in the surface SPM concentration data from MODIS because of the low number of cloud-free images during typhoon periods. Typhoons result in a short-term increase in the SPM concentration but do not strongly influence the seasonal values in satellite-derived SPM concentration maps.

Acknowledgments Part of this research is supported by the Ministry of Science and Technology (MOST105-2221-E-110-002). T.Y. Chou visited RBINS with a 2015 student abroad training fund granted by the Ministry of Education. M. Fettweis visited NSYSU with MOST and NSYSU scholar exchange funds. Part of the ocean seurface current data were retrieved 2015–05-07, from HYCOM https://hycom.org/data/glbu0pt08/expt-19pt1 HYCOM + NCODA Global 2015 1/12° reanalysis (GLBu0.08/expt_19.1).

References

Atlas R, Hoffman RN, Ardizzone J, Leidner SM, Jusem JC, Smith DK, Gombos D (2011) A cross-calibrated, multiplatform ocean surface wind velocity product for meteorological and oceanographic applications. Bull Am Meteorol Soc 92:157–174. doi:10.1175/2010BAMS2946.1

Bai Y, Huang T-H, He X, Wang S-L, Hsin Y-C, Wu C-R, Lui H-K, Chen C-TA (2015) Intrusion of the Pearl River plume into the main channel of the Taiwan Strait in summer. J Sea Res 95:1–15. doi:10.1016/j.seares.2014.10.003

Chen CTA, Wang S-L (2006) A salinity front in the southern East China Sea separating the Chinese coastal and Taiwan Strait waters from Kuroshio waters. Cont Shelf Res 26:1636–1653. doi:10.1016/j.csr.2006.05.003

Chien H, Chiang W-S, Cheng H-Y, Liu K-K (2011) On the resuspension of sediment in strong tidal current. Proc 33rd Ocean Eng Conf, National Kaohsiung Marine University, Taiwan

Cummings JA (2006) Operational multivariate ocean data assimilation. DTIC Document

Cummings JA, Smedstad OM (2013) Variational data assimilation for the global ocean. In: Data Assimilation for atmospheric, oceanic and hydrologic applications (Vol. II), p 303–343

Dadson S, Hovius N, Pegg S, Dade WB, Horng M, Chen H (2005) Hyperpycnal river flows from an active mountain belt. J Geophysi Res 110:F04016. doi:10.1029/2004JF000244

DeMaster DJ, McKee BA, Nittrouer CA, Jiangchu Q, Guodong C (1985) Rates of sediment accumulation and particle reworking based on radiochemical measurements from continental shelf deposits in the East China Sea. Cont Shelf Res 4:143–158

Dogliotti AI, Ruddick KR, Nechad B, Doxaran D, Knaeps E (2015) A single algorithm to retrieve turbidity from remotely-sensed data in all coastal and estuarine waters. Remote Sens Environ 156:157–168. doi:10.1016/j.rse.2014.09.020

Doxaran D, Froidefond J-M, Lavender S, Castaing P (2002) Spectral signature of highly turbid waters: application with SPOT data to quantify suspended particulate matter concentrations. Remote Sens Environ 81:149–161. doi:10.1016/S0034-4257(01)00341-8

Fettweis MP, Nechad B (2011) Evaluation of in situ and remote sensing sampling methods for SPM concentrations, Belgian continental shelf (southern North Sea. Ocean Dyn 61:157–171. doi:10.1007/s10236-010-0310-6

Fettweis M, Monbaliu J, Baeye M, Nechad B, Van den Eynde D (2012) Weather and climate induced spatial variability of surface suspended particulate matter concentration in the North Sea and the English Channel. Meth Oceanogr 3–4:25–39. doi:10.1016/j.mio.2012.11.001

Fox D, Teague W, Barron C, Carnes M, Lee C (2002) The Modular Ocean Data Assimilation System (MODAS). J Atmosph Ocean Technol 19:240–252

Han B, Loisel H, Vantrepotte V, Mériaux X, Bryère P, Ouillon S, Dessailly D, Xing Q, Zhu J (2016) Development of a semi-analytical algorithm for the retrieval of suspended particulate matter from remote sensing over clear to very turbid waters. Remote Sens 8:211. doi:10.3390/rs8030211

Hoefel F, Elgar S (2003) Wave-induced sediment transport and sandbar migration. Science 299:1885–1887

Hong H, Zhang C, Shang S, Huang B, Li Y, Li X, Zhang S (2009) Interannual variability of summer coastal upwelling in the Taiwan Strait. Cont Shelf Res 29:479–484. doi:10.1016/j.csr.2008.11.007

Jan S, Wang J, Chern C-S, Chao S-Y (2002) Seasonal variation of the circulation in the Taiwan Strait. J Mar Syst 35:249–268. doi:10.1016/S0924-7963(02)00130-6

Jan S, Wang Y-H, Wang D-P, Chao S-Y (2004) Incremental inference of boundary forcing for a three-dimensional tidal model: tides in the Taiwan Strait. Cont Shelf Res 24:337–351. doi:10.1016/j.csr.2003.11.005

Kao SJ, Milliman JD (2008) Water and sediment discharge from small mountainous rivers, Taiwan: the roles of lithology, episodic events, and human activities. J Geol 116:431–448. doi:10.1086/590921

Li Y, Xu X, Yin X, Fang J, Hu W, Chen J (2015) Remote-sensing observations of typhoon Soulik (2013) forced upwelling and sediment transport enhancement in the northern Taiwan Strait international. J Remote Sens 36:2201–2218. doi:10.1080/01431161.2015.1035407

Liao H-R, H-S Y, C-C S (2008) Morphology and sedimentation of sand bodies in the tidal shelf sea of eastern Taiwan Strait. Mar Geol 248:161–178. doi:10.1016/j.margeo.2007.10.013

Lin M-C, Juang W-J, Tsay T-K (2000) Applications of the mild-slope equation to tidal computations in the Taiwan Strait. J Oceanogr 56:625–642

Liu JT, Lin H-L, Hung J-J (2006) A submarine canyon conduit under typhoon conditions off southern Taiwan. Deep Sea Res I 53:223–240. doi:10.1016/j.dsr.2005.09.012

Liu Z, Tuo S, Colin C, Liu JT, Huang CY, Selvaraj K, Chen CTA, Zhao Y, Siringan FP, Boulay S, Chen Z (2008) Detrital fine-grained sediment contribution from Taiwan to the northern South China Sea and its relation to regional ocean circulation. Mar Geol 255:149–155. doi:10.1016/j.margeo.2008.08.003

Milliman JD, Kao SJ (2005) Hyperpycnal discharge of fluvial sediment to the ocean: impact of super-typhoon herb (1996) on Taiwanese rivers. J Geology 113:503–516

Milliman JD, Meade RH (1983) World-wide delivery of river sediment to the oceans. J Geol 91:1–21

NASA/GSFC/NOAA (2009) Cross-calibrated multi-platform ocean surface wind vector L3.0 first-look analyses. Ver. 1. PO.DAAC, CA, USA. Dataset accessed [2015–04-21] at 10.5067/CCF30-01XXX

Nechad B, Ruddick K, Park Y (2010) Calibration and validation of a generic multisensor algorithm for mapping of total suspended matter in turbid waters. Remote Sens Environ 114:854–866. doi:10.1016/j.rse.2009.11.022

Patt FS, Barnes R, Eplee R, Franz B, Robinson W (2003) Algorithm updates for the fourth SeaWiFS data reprocessing. NASA Technical Memorandum, 22

Qiu Y, Li L, Chen CA, Guo X, Jing C (2011) Currents in the Taiwan Strait as observed by surface drifters. J Oceanogr 67:395. doi:10.1007/s10872-011-0033-4

Schoellhamer DA (2002) Variability of suspended-sediment concentration at tidal to annual time scales in San Francisco Bay, USA. Cont Shelf Res 22:1857–1866. doi:10.1016/S0278-4343(02)00042-0

Song GS, Chen MP (1992) Grain size distributions and depositional processes in northern Taiwan Strait Hsin-Chu offshore area. Acta Oceanogr Taiwanica 13:84–108

Vanhellemont Q, Ruddick K (2011) Generalized satellite image processing: eight years of ocean colour data for any region on Earth. Proc SPIE 8175:81750Q. doi:10.1117/12.898300

Vanhellemont Q, Nechad, B, Ruddick, K (2011) GRIMAS: gridding and archiving of satellite-derived ocean colour data for any region on Earth. In: Longhorn R et al (eds) CoastGIS 5–8 September 2011 Oostende, Belgium, p 26–27

Wang YH, Jan S, Wang DP (2003) Transports and tidal current estimates in the Taiwan Strait from shipboard ADCP observations (1999–2001). Estuar Coast Shelf Sci 57:193–199. doi:10.1016/S0272-7714(02)00344-X

Wang P, Li Q, Li C-F (2014) Sedimentalogy. Geology of the China Seas, 1st edition. Elsevier. 301 pp

WRA (2016) Statistic of water resources. Water Resources Agency, Ministry of Economic Affairs. http://eng.wra.gov.tw/lp.asp?ctNode=6901&CtUnit=874&BaseDSD=4. Accessed 20 Jan 2016

Xu K, Milliman JD, Li A, Liu JP, Kao S-J, Wan S (2009) Yangtze-and Taiwan-derived sediments on the inner shelf of East China Sea. Cont Shelf Res 29:2240–2256. doi:10.1016/j.csr.2009.08.017

Yu H-C, Yu C-S, Chu C-H, Teyr T-C (2014) A regional ocean current forecast operational system for the sea around Taiwan. In: EGU Conf, 27 April–2 May, Vienna 5613